This document is confidential and is proprietary to the American Chemical Society and its authors. Do not copy or disclose without written permission. If you have received this item in error, notify the sender and delete all copies.

Synthesis of Synergistic N-doped NiMoO4/Ni3N Heterostructure for Implementation of An Efficient Alkaline Electrocatalytic Hydrogen Evolution Reaction

Journal:	*ACS Applied Energy Materials*
Manuscript ID	ae-2019-021304.R1
Manuscript Type:	Article
Date Submitted by the Author:	15-Jan-2020
Complete List of Authors:	Liu, Xiaolei; State Key Lab of Crystal Materials, Shandong University Guo, Yuhao; State Key Lab of Crystal Materials, Shandong University Wang, Peng; State Key Lab of Crystal Materials, Shandong University Wu, Qian; Shandong University, School of Physics Zhang, Qianqian; State Key Lab of Crystal Materials, Shandong University Rozhkova, Elena; Argonne National Laboratory, Center for Nanoscale Materials Wang, Zeyan; State Key Lab of Crystal Materials, Shandong University Liu, Yuanyuan; State Key Lab of Crystal Materials, Zheng, Zhaoke; Shandong University, State Key Laboratory of Crystal Materials Dai, Ying; Shandong University, School of Physics Huang, Baibiao; State Key Lab of Crystal Materials, Shandong University

SCHOLARONE™
Manuscripts

Synthesis of Synergistic N-doped $NiMoO_4/Ni_3N$ Heterostructure for Implementation of An Efficient Alkaline Electrocatalytic Hydrogen Evolution Reaction

Xiaolei Liu,[†,∇] Yuhao Guo,[†,∇] Peng Wang,[*,†] Qian Wu,[‡] Qianqian Zhang,[†] Elena A. Rozhkova,[§] Zeyan Wang,[†] Yuanyuan Liu,[†] Zhaoke Zheng,[†] Ying Dai,[‡] and Baibiao Huang[†]

[†]State Key Lab of Crystal Materials, Shandong University, Jinan 250100, China

[‡]School of Physics, Shandong University, Jinan 250100, China

[§]Center for Nanoscale Materials, Argonne National Laboratory, 9700 South Cass Avenue, Argonne, Illinois 60439-4855, United States

ABSTRACT: Electrochemical water splitting is considered as an effective and promising method to produce the ideal hydrogen energy to solve the energy crisis and environmental pollution problems. Herein, we successfully synthesized the N-doped $NiMoO_4/Ni_3N$ heterostructure, which exhibited an efficient HER performance with a lower overpotential of 51 mV at 10 mA cm^{-2} and a lower Tafel slope value of 45.47 mV dec^{-1} compared with those of $NiMoO_4$, N-doped $NiMoO_4$ or Ni_3N owing to the synergistic effect of N doping and construction of the superior heterostructure. When the N-doped $NiMoO_4/Ni_3N$ heterostructure is used as a cathode and the well-recognized excellent OER material (NiFe-LDH) is used as an anode to construct the two-electrode electrolyzer, the system requires only 1.506 and 1.559 V to achieve the current density of 10 and 20 mA cm^{-2}, respectively, which are lower than those of commercial Pt/C//RuO_2 system (1.573 and 1.634 V, respectively) or many other reported systems. At the same time, this two-electrode system demonstrates excellent durability in electrocatalytic water splitting. This design method paved the way for the development of other electrocatalytic system.

KEYWORDS: electrocatalyst, hydrogen evolution reaction, heterostructure, N doping, synergistic, Ni_3N

INTRODUCTION

Electrochemical water splitting as a promising method for the production of high energy density, renewable and clean hydrogen fuel for replacing traditional fossil fuels has received close attention due to its clean, pollution-free characteristics, and easy separation and collection of the generated gas.[1-4] Platinum (Pt) and Pt-based materials are recognized as the most efficient electrocatalysts for hydrogen production with a near-zero overpotential, however, their high cost and low supply limit their large-scale practical application.[5-8] After years of intensive research and development, many cost-efficient and abundant HER electrocatalysts have been explored, such as transition metal sulfides,[9-11] nitrides,[12-14] phosphides,[15-17] oxides,[18-20] borides[21,22] and so on. Although they exhibit a certain degree of electrocatalytic hydrogen evolution activities, their characteristics are still far from satisfaction due to the large gap with the excellent performance of the precious metal Pt. Therefore, it is very important to develop more effective strategies to improve their electrocatalytic hydrogen evolution performances, which can reduce the energy losses during electrocatalytic water splitting.

Doping is one of the effective strategies for improving the electrocatalytic HER performance, which can enhance the conductivity, adjust the electronic structure and increase the number of active catalytic sites. Doping strategy may involve metal ion doping and non-metal ion doping, and both approaches have been reported in electrocatalytic HER application. For example, Feng's group reported that Ni-doped MoS_2 nanosheets showed higher HER activity than the un-doped MoS_2 with an extremely low overpotential of 98 mV at 10 mA cm^{-2} in 1 M KOH aqueous solution, which can be explained by improved conductivity, lower kinetic energy barrier of the initial water dissociation step and facilitated desorption of the formed OH^- from the surface of the catalyst, which are beneficial for improving the HER activity.[23] Chen et al. reported that the V-doped Co_4N nanosheets displayed a significantly higher HER activity than the pristine Co_4N with an low overpotential of 37 mV at 10 mA cm^{-2}, and the increased HER activity is attributed to the downshift of the d-band center

caused by V doping, which can accelerate the desorption of the H-intermediate.[24] Yan et al. reported the synthesis of N-doped MoO_2 using urea as the nitrogen source and reducing agent, which exhibited excellent Pt-like HER performance; the superior activity was attributed to doping-induced disorder of the surface lattice, which could therefore increase the number of active sites for proton adsorption and reducing the binding strength between the H intermediate and the catalyst.[25]

Construction of heterostructure is another effective strategy for improving the electrocatalytic HER performance, which can support abundant active sites, optimize the surface and interfacial properties of electrocatalyst (such as hydrogen or water adsorption energy) to accelerate the kinetic process of electrocatalytic HER and reduce the charge-transfer resistance. For example, Xiao et al. synthesized the low-cost NiS/Ni_2P heterostructures as electrocatalyst, which exhibited improved HER performance compared to NiS or Ni_2P alone due to the abundant active sites, smaller charge-transfer resistance and stronger electronic interactions in the NiS/Ni_2P heterostructure system.[26] Pan's group reported on experimental and DFT calculation results demonstrating the Ni_2P/Ni_3S_2 heterostructure with significantly increased HER electrocatalytic activity due to the strong interaction between Ni_2P and Ni_3S_2, which can optimize the electronic structure and regulate the Gibbs free energies of hydrogen and water adsorption on the catalyst surface.[27] Recently, our group reported on the design and synthesis of $Co(OH)_2/MoS_2$ heterostructure, which demonstrated significantly improved electrocatalytic HER performance compared to that of MoS_2 or $Co(OH)_2$ due to the excellent synergistic effects of the heterogeneous interface.[28]

Thus, according to the above discussion both doping and construction of heterostructure strategies are useful for the improvement of electrocatalytic HER performance. Herein, we combined doping and heterostructure construction strategies to synthesize the N-doped $NiMoO_4/Ni_3N$ heterostructure, which exhibits a good HER performance with a lower overpotential of 51 mV at 10 mA cm^{-2} and a lower Tafel slope value of 45.47 mV dec^{-1} compared with those of $NiMoO_4$, N-doped $NiMoO_4$ or Ni_3N. The HER performance of the N-doped $NiMoO_4/Ni_3N$ heterostructure is better than that of many reported HER electrocatalysts, and when it is combined with the

NiFe-layered double hydroxide (NiFe-LDH) which is recognized as the best OER electrode to construct a two-electrode electrolysis system, only low cell voltages 1.506 V and 1.559 V are required to achieve the current densities of 10 and 20 mA cm^{-2}, respectively, and it has a good stability for overall water splitting, surpassing most reported electrolyzers. Combining the experimental results and DFT calculation, we propose a reasonable explanation for the improvement in the HER performance of N-doped $NiMoO_4/Ni_3N$ heterostructures. This work indicates that the synergistic effect of combining doping with the construction of heterostructures strategies can play an important role in the synthesis of the excellent HER electrocatalyst.

EXPERIMENTAL SECTION

Materials. Nickel nitrate hexahydrate ($Ni(NO_3)_2 \cdot 6H_2O$), ammonium molybdate tetrahydrate ($(NH_4)_6Mo_7O_{24} \cdot 4H_2O$), iron nitrate nonahydrate ($Fe(NO_3)_3 \cdot 9H_2O$), urea, ammonium fluoride (NH_4F), ammonium hydroxide ($NH_3 \cdot H_2O$) and potassium hydroxide (KOH) were purchased from Sinopharm Chemical Reagent Co. Ltd. Ni foam (NF) was purchased from Lizhiyuan company, China, it was cut into pieces 2 × 3.5 cm^2 in size and cleaned by sonication in acetone, ethanol, 3 M HCl and DI water (15 min each), respectively. All the reagents were of analytical grade without further purification and the deionized water was used throughout the experiment.

Synthesis of the $NiMoO_4$ electrode. 1.2 mmol $Ni(NO_3)_2 \cdot 6H_2O$ and 0.3 mmol $(NH_4)_6Mo_7O_{24} \cdot 4H_2O$ were dissolved in 30 mLH_2O, and the pH of the above solution was adjusted to 7.0 using ammonium hydroxide. Then a piece of Ni foam (2 cm × 3.5 cm) was placed into the solution and they were transferred into a 40 mL Teflon-lined stainless steel autoclave and maintained at 150 °C for 6 h. When cooled to room temperature, the as-prepared electrode was removed and washed by water and ethanol for several times, after drying, the as-prepared electrode was annealed in air at 450 °C for 3 h to obtain the $NiMoO_4$ electrode.

Synthesis of the N-doped $NiMoO_4$ electrode. A piece of $NiMoO_4$ electrode was placed in a crucible, then put the crucible in the middle of the tube furnace and heated to 380 °C for 3 h with a rate of 10 °C min^{-1} under NH_3 flow. The cooling process was

also carried out under the NH_3 atmosphere, the as-prepared N-doped $NiMoO_4$ was used to synthesize the N-doped $NiMoO_4/Ni_3N$. The as-prepared N-doped $NiMoO_4$ was further heated to 380 °C for 1 h with a rate of 10 °C min^{-1} under NH_3 flow in the tube furnace, which can obtain the final N-doped $NiMoO_4$ used for the comparison of HER performance.

Synthesis of the N-doped $NiMoO_4/Ni_3N$ and Ni_3N electrodes. In order to synthesize of the N-doped $NiMoO_4/Ni_3N$ electrode, the N-doped $NiMoO_4/Ni(OH)_2$ precursor was synthesized by the electrodeposition method in a standard three-electrode system (the as-prepared N-doped $NiMoO_4$ as a working electrode, a carbon electrode as a counter electrode, an Ag/AgCl (saturated KCl) electrode as a reference electrode and an electrolyte was 0.1 M $Ni(NO_3)_2 \cdot 6H_2O$ aqueous solution). The potentiostatic electrodeposition process was carried out at a bias of -1.0 V vs. Ag/AgCl, the electric charge pass through the cell with the formation of $Ni(OH)_2$ on the working electrode, while the passed electric charge was 7 Coulombs (C), the contrast experiments used 3 C, 5 C and 10 C. Then the as-prepared working electrode was rinsed with deionized water and alcohol, and dried, the N-doped $NiMoO_4/Ni(OH)_2$ precursor was placed in a crucible at the middle of a tube and then the tube was heated to 380 °C for 1 h in a tube furnace with a rate of 10 °C min^{-1} under NH_3 flow. After natural cooling in an NH_3 atmosphere, the N-doped $NiMoO_4/Ni_3N$ electrode was obtained. The Ni_3N electrode was synthesized using the same electrodeposition and nitriding process except the working electrode (as-prepared N-doped $NiMoO_4$) was replaced by the cleaned Ni foam.

Synthesis of the NiFe-LDH. In a typical synthesis process, 1.2 mmol $Ni(NO_3)_2 \cdot 6H_2O$, 0.4 mmol $Fe(NO_3)_3 \cdot 9H_2O$ and 8 mmol urea were dissolved in 32 mL H_2O, then 3.2 mmol NH_4F was placed to the above solution and stirred for 30 min. A piece of Ni foam (2 cm × 3.5 cm) was placed to the above solution and they were transferred to a 40 mL Teflon-lined stainless steel autoclave and maintained at 120 °C for 6 h. After cooling down to room temperature, the as-prepared NiFe-LDHs electrode was removed, washed by water and ethanol for several time and dried at 60 °C for 3 h.

Materials characterization. X-ray powder diffraction (XRD) patterns were recorded by the Bruker AXS D8 diffractometer equipped with Cu Kα radiation (λ = 0.154056 nm), the morphologies and microstructures of the samples were observed by scanning electron microscopy (SEM, Hitachi S-4800) and transmission electron microscopy (TEM, JEOL JEM-2100F). X-ray photoelectron spectroscopy measurements were performed by Thermo Fisher Scientic Escalab 250 spectrometer to study the surface chemical states of the samples and corrected by C 1s line at 284.6 eV.

Electrochemical measurements. All the electrochemical measurements were conducted with a CHI 660E electrochemical workstation in a standard three-electrode system (the as-prepared samples (the size of 1 × 3 cm^2) were directly used as the working electrodes with the working area of 1 × 1 cm^2 immersed in the electrolyte for testing, a graphite rod was used as the counter electrode and Hg/HgO (1.0 M KOH) was used as the reference electrode, respectively) and the electrolyte was 1 M KOH (pH = 13.8). All the corresponding potential values were converted to the reversible hydrogen electrode (RHE) according to the formula: $E_{RHE} = E_{Hg/HgO} + 0.0591 \times pH + 0.098$. Before the formal measurement, the working electrode needed to be pre-activated by 25 cyclic voltammetric sweeps from 0 to -0.4 V with a scan rate of 50 mV s^{-1}. The polarization curves were measured by linear sweep voltammetry (LSV) at a scan rate of 2 mV s^{-1} (the fast scan speed can't get the accurate test results) and iR corrected by the electrochemical workstation, electrochemical impedance spectroscopy (EIS) was measured with frequency ranging from 100 KHz to 0.1 Hz, AC voltage of 10 mV at -120 mV (to compare the charge transfer capability of the sample during the HER). The electrochemical double layer capacitance (C_{dl}) was determined by the cyclic voltammetry measurement in the non-faradaic region from 0.05 to 0.15 V vs. RHE with different scan rates from 3 to 12 mV s^{-1} to study the electrochemical active area. The C_{dl} was obtained by plotting the figure of $j = j_{anodic} - j_{cathodic}$ at 0.1 V vs. RHE against the scan rate, and the linear slope was twice the C_{dl}. The stability was verified by the cyclic voltammetry circulation measurement and long-term potentiostatic test (I-T curve without iR-compensation). The overall water

splitting measurement was performed in a two-electrode system by using the NiFe-LDH as anode and N-doped $NiMoO_4/Ni_3N$ as cathode, and the polarization curves were obtained by LSV without iR-compensation at a scan rate of 2 mV s^{-1}. The corresponding commercial 20 wt% Pt/C and RuO_2 powder were dipped on Ni foam for the comparison experiment.

RESULTS AND DISCUSSION

In order to study the structure of the electrodes, the XRD spectra of the as-prepared samples scraped off Ni foam by ultrasound were obtained, and the results are shown in Figure 1. Figure 1a shows that the diffraction peaks of as-prepared $NiMoO_4$ were consistent with those of the standard PDF card of $NiMoO_4$ (no. 33-0948), thus, this result indicates that the successful synthesis of $NiMoO_4$.[29,30] After calcination treatment under an NH_3 atmosphere, the XRD spectrum of as-prepared N-doped $NiMoO_4$ was almost the same as that of the as-prepared $NiMoO_4$, which indicates that the N doping did not affect the overall crystal structure of $NiMoO_4$. In Figure 1b, the XRD spectrum of as-prepared N-doped $NiMoO_4/Ni_3N$ contained the diffraction peaks of N-doped $NiMoO_4$ and Ni_3N (JCPDS no. 89-5144),[31] which proved that the N-doped $NiMoO_4/Ni_3N$ heterostructure was successfully synthesized.

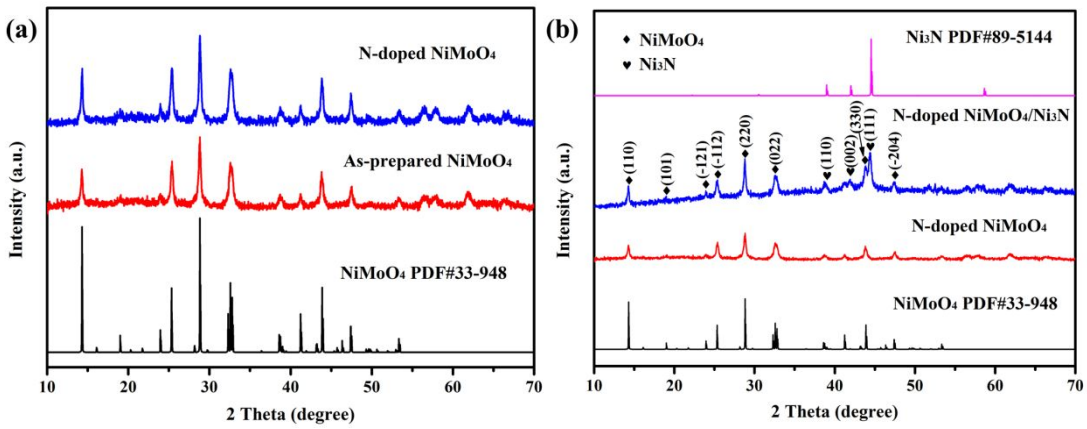

Figure 1. (a) XRD patterns of as-prepared $NiMoO_4$ and N-doped $NiMoO_4$, (b) XRD patterns of N-doped $NiMoO_4$ and N-doped $NiMoO_4/Ni_3N$ heterostructure.

The morphologies and microstructures of the as-prepared samples were observed by SEM and the surface of the original Ni foam was smooth as can be seen in Figure S1a. SEM image of as-prepared $NiMoO_4$, as presented in Figure 2a, shown that its

morphology is consist of nanowires. Figure 2b shown that the morphology of N-doped $NiMoO_4$ was almost no change compared with that of the as-prepared $NiMoO_4$, which indicated that N-doping does not affect its microstructure. SEM images of electrodeposited $Ni(OH)_2$, Figure S1b, and Ni_3N obtained from the nitridation of $Ni(OH)_2$, Figure 2c, show that they are composed of irregular nanoparticles. As it can be seen from SEM images of a heterostructure presented in Figure 2d-f, the N-doped $NiMoO_4/Ni_3N$ composite fully and densely covers the Ni foam substrate thus preserving the nanowire-like morphology, while nanowires become thicker and coarser compared to that of the N-doped $NiMoO_4$ owing to the healing effect of Ni_3N loading.

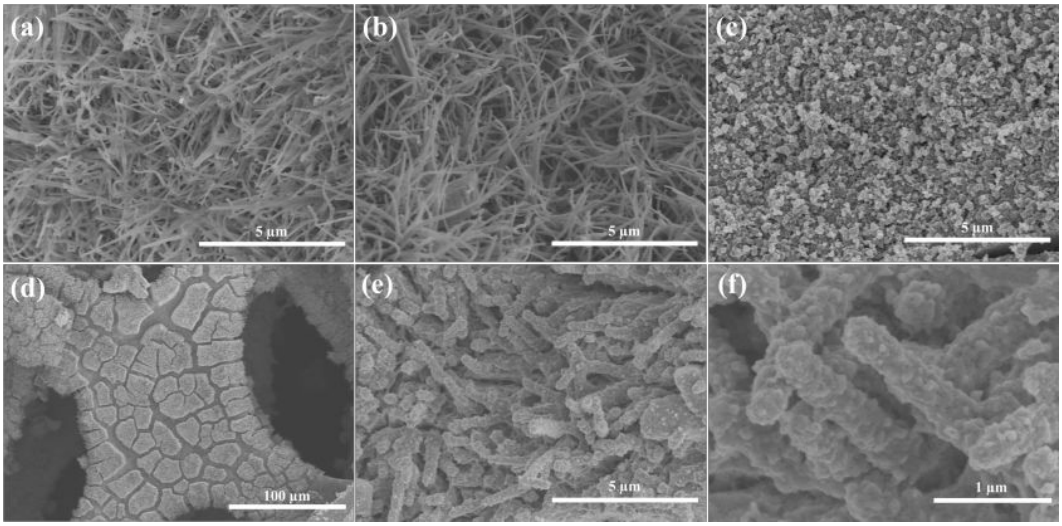

Figure 2. The SEM images of as-prepared $NiMoO_4$ (a), N-doped $NiMoO_4$ (b), Ni_3N (c) and N-doped $NiMoO_4/Ni_3N$ heterostructure (d-f).

In order to provide further insights regarding the microstructure and morphology of the N-doped $NiMoO_4/Ni_3N$ heterostructure, the TEM characterization was carried out. As shown in Figure 3a and b, the N-doped $NiMoO_4/Ni_3N$ heterostructure is nanowires whose surface is covered by small nanoparticles, which is consistent with the SEM result. From the HRTEM images shown in Figure 3c and d, the lattice fringes with a spacing of about 0.356 nm can be assigned to the (-112) crystal plane of $NiMoO_4$,[32] while the lattice fringes with spacing of 0.237 nm and 0.214 nm are assigned to the (110) and (002) crystal planes of Ni_3N,[31,33] respectively. Thus, we can conclude that the TEM results further prove that the N-doped $NiMoO_4/Ni_3N$ heterostructure is

successfully synthesized.

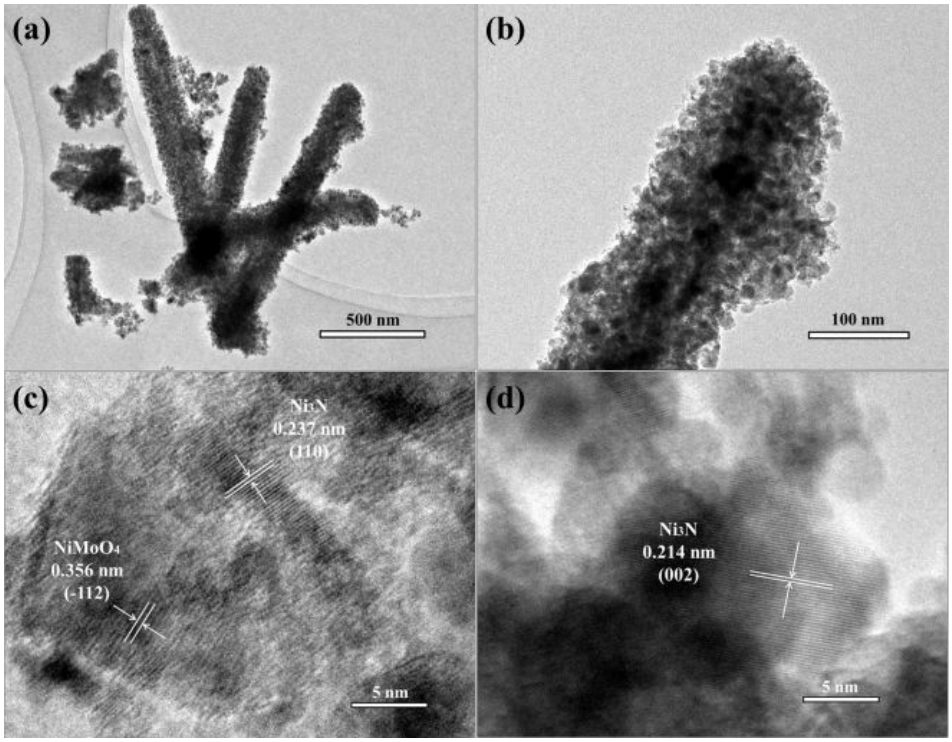

Figure 3. The TEM images (a, b) and HRTEM images (c, d) of N-doped $NiMoO_4/Ni_3N$ heterostructure.

The surface chemical composition and elemental valence states of the as-prepared samples were analyzed by the X-ray photoelectron spectroscopy (XPS). From Figure S5 and S6 (XPS results of pristine $NiMoO_4$ and N-doped $NiMoO_4$), it can be seen that N element was successfully doped into the $NiMoO_4$ and the low valence Mo and oxygen vacancy were appeared during the N doping under NH_3 atmosphere. Figure 4 shows the presence of Ni, Mo, O and N elements on the surface of the N-doped $NiMoO_4/Ni_3N$ heterostructure. Figure 4a shows the high resolution XPS spectrum of Ni 2p, the peaks located at 852.85 eV and 870.45 eV belong to Ni^+ in Ni_3N,[34,35] the peaks located at 855.55 eV and 873.55 eV relate to Ni^{2+} $2p_{3/2}$ and Ni^{2+} $2p_{1/2}$ in N-doped $NiMoO_4$, respectively,[36] while two satellite peaks of Ni are located at 861.7 eV and 879. 95 eV, respectively.[7] Figure 4b shows the high resolution XPS spectrum of Mo 3d, there are three valence states (+4, +5 and +6) in N-doped $NiMoO_4$ due to the reductive nature of NH_3 during nitridation. The peaks located at 235.25 eV and 232 eV are ascribed to Mo^{6+}, the peaks located 233.1 eV and 229.8 eV are ascribed to Mo^{5+}, and the peaks located at 232.35 eV and 228.9 eV are ascribed to Mo^{4+}.[36] Figure

4c shows the high resolution XPS spectrum of N 1s, the regions of N 1s and Mo 3p have partial overlap, the peak located at 395.25 eV is attributed to Mo $3p_{3/2}$, the peaks located at 395.25 eV and 398.85 eV are ascribed to Ni-N and N-H species, which indirectly proved the successful synthesis of Ni_3N. Figure 4d shows the high resolution XPS spectrum of O 1s, where the three peaks located at 530.35 eV, 531.9 eV and 532.95 eV are attributed to lattice oxygen, oxygen vacancy and chemisorbed oxygen species, respectively, that proves the existence of oxygen vacancy which is favorable for the electroctalytic HER performance.[37] Altogether, the XPS results show that the N-doped $NiMoO_4/Ni_3N$ heterostructure with properties suitable for efficient HER was successfully prepared.

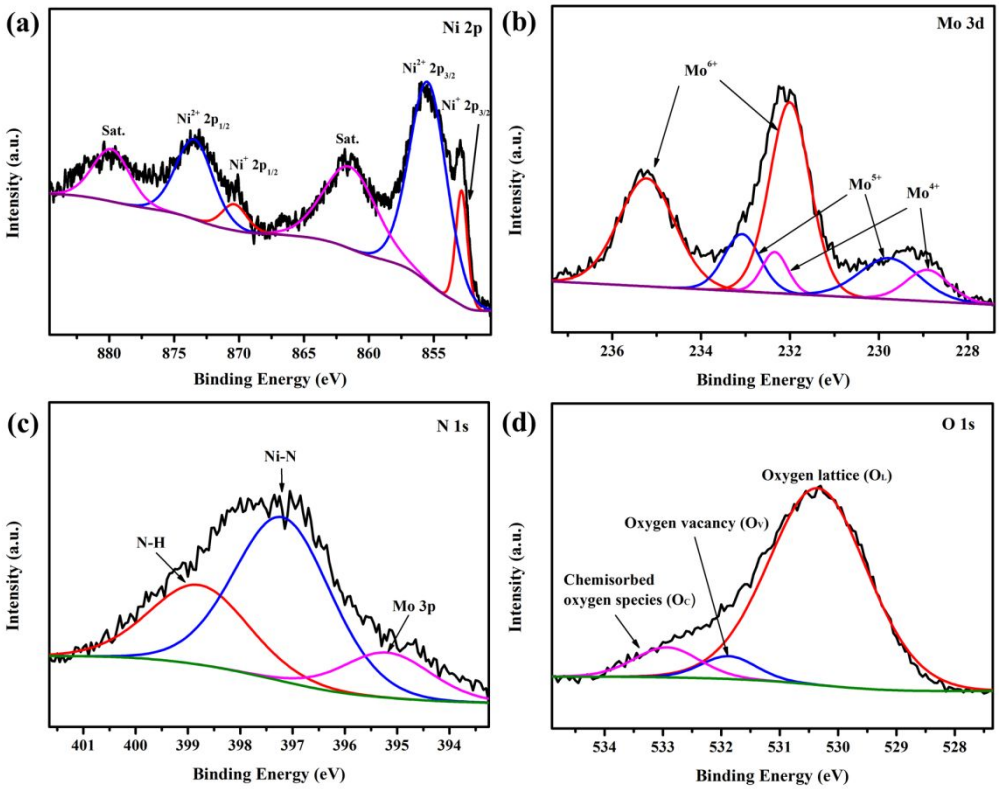

Figure 4. The high resolution XPS spectra of the Ni 2p region (a), Mo 3d region (b), N 1s region (c) and O 1s region (d) in N-doped $NiMoO_4/Ni_3N$ heterostructure.

The electrocatalytic HER performances of Ni foam, $NiMoO_4$, N-doped $NiMoO_4$, Ni_3N and N-doped $NiMoO_4/Ni_3N$ heterostructure were measured in a typical three-electrode system in 1 M KOH solution at room temperature. Linear sweep voltammetry (LSV) measurements were carried out firstly to evaluate the HER

performances of the as-prepared samples, as shown in Figure 5a (iR-corrected polarization curves). The $NiMoO_4$ electrode exhibits negative HER activity with the overpotential of 275 mV at 10 mA cm^{-2}, while the N-doped $NiMoO_4$ electrode shows superior and significantly improved HER performance compared to the original $NiMoO_4$ electrode with the overpotential of 61 and 149 mV at 10 and 100 mA cm^{-2}, respectively. Construction of N-doped $NiMoO_4/Ni_3N$ heterostructure exhibits further enhanced and optimal HER activity with the overpotential of 51 and 112 mV at 10 and 100 mA cm^{-2}, respectively, which is better than that of N-doped $NiMoO_4$ or Ni_3N (with the overpotential of 165 and 286 mV at 10 and 100 mA cm^{-2}, respectively), while the effect of Ni_3N loading amount on HER performance can be seen in Figure S2. In order to study the dominant HER mechanism, rate-limiting step and HER kinetics of the as-prepared samples, the corresponding Tafel plots were obtained according to the Tafel equation ($\eta = b \times \log |j| + a$), where η is the overpotential, j is the current density, b is the Tafel slope and a is a constant,[7,28] as shown in Figure 5b. The Tafel slope values of $NiMoO_4$, Ni_3N and N-doped $NiMoO_4$ are 124.23, 117.9 and 54.34 mV/dec, respectively, while the N-doped $NiMoO_4/Ni_3N$ heterostructure exhibits a lower Tafel slope value of 45.57 mV/dec, which indicates that N doping and construction of N-doped $NiMoO_4/Ni_3N$ heterostructure can promote the HER kinetic process. According to the classic theory for alkaline HER, when the Tafel slope is about 120 mV/dec, the Volmer reaction ($H_2O + e^- \rightarrow H_{ads} + OH^-$) containing dissociation of water and adsorption of hydrogen intermediate is the rate-determining step; when the Tafel slope is about 40 or 30 mV/dec, the Heyrovsky reaction ($H_2O + H_{ads} + e^- \rightarrow OH^- + H_2$) or Tafel reaction ($H_{ads} + H_{ads} \rightarrow H_2$) containing the desorption and aggregation of hydrogen intermediate is the rate-determining step, respectively.[38] The Tafel slope values of Ni_3N, N-doped $NiMoO_4$ and N-doped $NiMoO_4/Ni_3N$ heterostructure are within the range of 40-120 mV/dec, demonstrating that a combined Volmer-Heyrovsky mechanism for HER with the desorption and aggregation of hydrogen intermediate as a rate-determining step during HER.[28] The exchange current density (j_0) was calculated using the extrapolation method based on Tafel equation, as shown in Figure 5c, which can reflect the intrinsic electrochemical

HER activity.[39] The exchange current density (j_0) values of $NiMoO_4$, Ni_3N, N-doped $NiMoO_4$ and N-doped $NiMoO_4/Ni_3N$ heterostructure are 0.0674, 0.425, 0.716 and 1.03 mA cm^{-2}, respectively, N-doped $NiMoO_4/Ni_3N$ heterostructure has the largest exchange current density (j_0), which indicates that it has the most favorable intrinsic HER rate. A comparison of this HER activity with that of recently reported for other HER electrocatalysts is presented in Table S1, which demonstrates that the N-doped $NiMoO_4/Ni_3N$ heterostructure outperforms most reported HER electrocatalysts. The electrochemical impedance spectroscopy (EIS) test was carried out at -120 mV vs. RHE to evaluate the ability of charge transfer during HER, as shown in Figure S3, N-doped $NiMoO_4/Ni_3N$ heterostructure has the lowest charge transfer resistance and the optimal charge transfer ability, which is important for the efficient HER. Electrochemically active surface areas (ECSA) can reflect the number of HER active sites, which is related to the HER activity. The ECSA is linearly proportional to the electrochemical double-layer capacitance (C_{dl}), so the value of C_{dl} can stand for the value of ECSA.[40] As shown in Figure S4 and Figure 5d, the $NiMoO_4$ and Ni_3N have the lowest values of C_{dl} (3.66 and 34.94 mF cm^{-2}, respectively) which lead to their low HER activity; while the N-doped $NiMoO_4$ shows a significantly improved value of C_{dl} (327.21 mF cm^{-2}) and finally construction of N-doped $NiMoO_4/Ni_3N$ heterostructure has the largest value of C_{dl} (339.42 mF cm^{-2}), indicating that N doping and construction of N-doped $NiMoO_4/Ni_3N$ heterostructure can increase the ECSA thus supplying more HER active sites, that are beneficial to the HER activity. Besides, stability is also a very important parameter of a HER electrode; an ideal electrode should combine excellent HER activity and stability. Evaluation of stability carried out by cyclic voltammetry (CV) and chronoamperometry (CA) as can be seen in Figure 5e, showed that the HER activity of N-doped $NiMoO_4/Ni_3N$ heterostructure was not attenuated but had a slight increase after 3000 continuous CV cycles from 0.05 to -0.35 V vs. RHE with a scan rate of 100 mV s^{-1}. In order to study the reason for the enhanced HER activity after 3000 continuous CV cycles, XPS measurement was carried out, the result is shown in Figure S7. All the surface chemical compositions and elemental valence states of the N-doped $NiMoO_4/Ni_3N$

heterostructure after 3000 continuous CV cycles remain virtually unchanged relative to the initial N-doped $NiMoO_4/Ni_3N$ heterostructure except that the peak intensity of Ni^+ in Ni_3N becomes lower, which means that part of the Ni_3N must be oxidized to nickel oxide or hydroxide (Ni^{2+}) during HER stability test. This is consistent with some reports proving that the formation of transition metal oxide or hydroxide is beneficial to alkaline HER.[41-43] In addition, the CA test (Figure 5f, without iR-compensation) was done at -79 mV vs. RHE to get the current density of about 10 mA cm^{-2} (actually, the current density is reached 15 mA cm^{-2}), which is the current density expected for a 12.3% efficient solar water-splitting device. The result shows that the current density practically does not deteriorate after 24-hours electrolysis. The XRD pattern of the sample after cycle test shown in Figure S8 demonstrates that the structure of N-doped $NiMoO_4/Ni_3N$ heterostructure is preserved except that the intensity of the Ni_3N diffraction peak is weakened, which agrees with the above XPS result. Analogously, as shown in the SEM images of the sample after the test cycle, presented in Figure S9, the morphology is practically unchanged compared to the original sample. All of the above results prove that the N-doped $NiMoO_4/Ni_3N$ heterostructure has superior HER activity and structural stability.

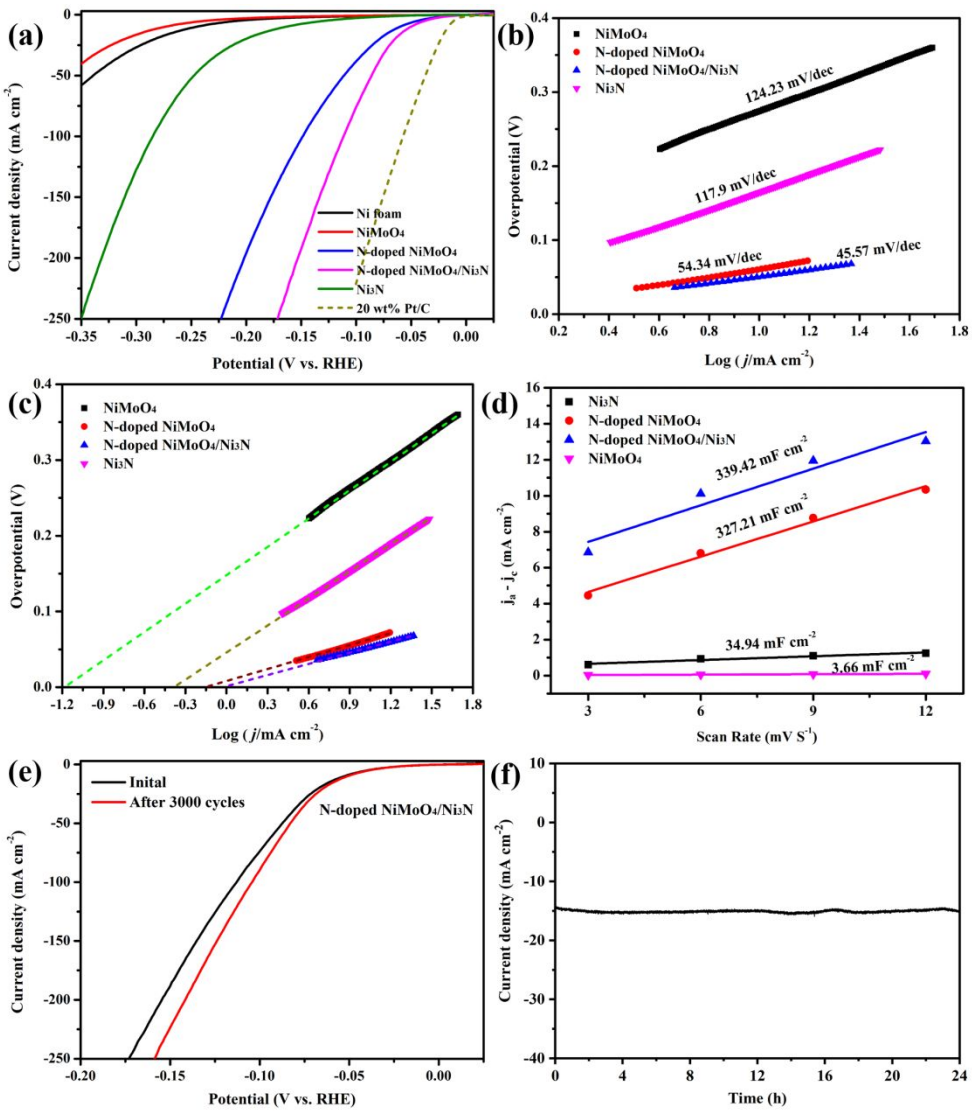

Figure 5. (a-c) Polarization curves, the corresponding Tafel slopes and the exchange current density (j_0) of Ni foam, $NiMoO_4$, N-doped $NiMoO_4$, Ni_3N and N-doped $NiMoO_4/Ni_3N$ heterostructure. (d) The C_{dl} of the different samples obtained at 0.1 V vs. RHE. (e) Polarization curves of N-doped $NiMoO_4/Ni_3N$ heterostructure before and after 3000 continuous CV cycles from 0.05 to -0.35 V vs. RHE with a scan rate of 100 mV s^{-1}. (f) Chronoamperometry measurement without iR-compensation (at -79 mV vs. RHE) of the N-doped $NiMoO_4/Ni_3N$ heterostructure.

To further understand the reason for the superior HER performance of N-doped $NiMoO_4/Ni_3N$ heterostructure, density functional theory (DFT) modeling was carried out. As shown in Figure S10 (total and partial DOS for pristine $NiMoO_4$ and N-doped $NiMoO_4$), we can see that N-doped $NiMoO_4$ exhibits a significantly reduced band gap, indicating that N doping can significantly improve the conductivity of $NiMoO_4$

and facilitate carrier transport. At the same time, N doping can generate more active sites on the surface of $NiMoO_4$ proved by the ECSA result. According to the above discussions, the N doping can significantly improve the HER performance of $NiMoO_4$. As previously reported, metal oxides generally have good hydrophilicity that benefits the adsorption and dissociation of water on their surface in alkaline solution.[43-45] Ni_3N is regarded as the promising candidate for HER due to its excellent conductivity and chemical stability, however, its alkaline HER activity is not satisfactory due to its low efficiency in splitting water into hydrogen intermediates.[42] When N-doped $NiMoO_4$ and Ni_3N are combined to form the heterostructure, a superior heterogeneous interface can facilitate the decomposition of water, optimize the adsorption and desorption of hydrogen intermediates and further increase number of reactive sites, at the same time, good conductivity of the heterostructure is beneficial for promoting carrier transport and transfer, which should be the reason for its superior HER activity.

In order to verify the actual electrolyzed water capacity of N-doped $NiMoO_4/Ni_3N$ heterostructure, we constructed the two-electrode electrolyzer using N-doped $NiMoO_4/Ni_3N$ heterostructure as cathode, and hydrothermally synthesized NiFe-LDH as anode which is recognized as an excellent OER electrocatalyst with the high intrinsic activity and low OER overpotential.[46,47] The corresponding characterizations of the as-synthesized NiFe-LDH electrode can be seen in Figure S11, the NiFe-LDH electrode showed excellent OER performance which is better than that of commercial RuO_2. For comparison, we also prepared the commercial Pt/C and RuO_2 electrodes with the same loading amount using as cathode and anode, respectively. The electrocatalytic water splitting activities of the samples can be seen in Figure 6a, the N-doped $NiMoO_4/Ni_3N$//NiFe-LDH system exhibits more superior electrocatalytic water splitting activity than that of commercial Pt/C//RuO_2 system. The N-doped $NiMoO_4/Ni_3N$//NiFe-LDH system only needs 1.506 and 1.559 V to reach the current density of 10 and 20 mA cm^{-2}, respectively, which are lower than those of commercial Pt/C//RuO_2 system (1.573 and 1.634 V, respectively) or many other reported systems (Table S2). Figure 6b shows that the system exhibited good electrolyzed water

stability, and the current density almost had no attenuation for 50 h at the voltage of 1.535 V. In order to satisfy the potential application in industry, we also do the HER and overall water splitting stability tests in higher concentrations of KOH (2.5 M and 5.0 M). As shown in Figure S12 and 13, they all demonstrate the good stability during water splitting. The above results show that this electrode material has good application prospects in electrocatalytic water splitting.

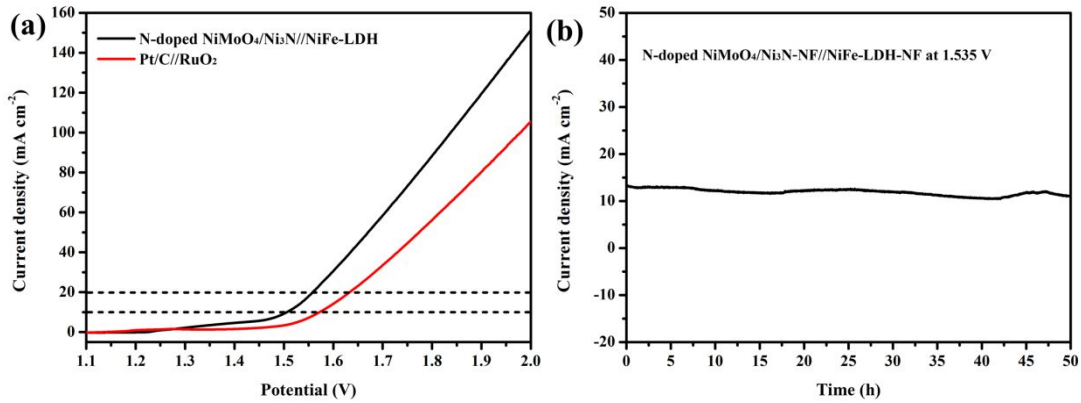

Figure 6. (a) LSV curves of N-doped $NiMoO_4/Ni_3N$//NiFe-LDH and commercial Pt/C//RuO_2 systems in 1 M KOH solution without iR correction. (b) The stability tests of N-doped $NiMoO_4/Ni_3N$//NiFe-LDH system at the voltage of 1.535 V without iR correction.

CONCLUSIONS

In summary, our work demonstrate that the N-doped $NiMoO_4/Ni_3N$ heterostructure is a superior HER electrocatalyst. N doping in $NiMoO_4$ can significantly reduce its band gap and improve its conductivity, which can promote carrier transport and transfer. At the same time, N doping can generate more active sites on the surface of $NiMoO_4$, which is beneficial to HER. Construction of heterostructure to supply the superior heterogeneous interface can facilitate the decomposition of water, optimize the adsorption and desorption of hydrogen intermediates and further increase the reactive sites. The synergistic effect of combining doping strategy with construction of heterostructure strategy realize the efficient HER performance of N-doped $NiMoO_4/Ni_3N$ heterostructure with a lower overpotential of 51 mV at 10 mA cm^{-2} and a lower Tafel slope value of 45.47 mV dec^{-1} compared with those of $NiMoO_4$,

N-doped $NiMoO_4$ or Ni_3N. When N-doped $NiMoO_4/Ni_3N$ heterostructure combined with the well-recognized excellent OER material (NiFe-LDH) in a two-electrode electrolyzer, the N-doped $NiMoO_4/Ni_3N$//NiFe-LDH system only need 1.506 and 1.559 V to reach the current density of 10 and 20 mA cm^{-2}, respectively, which are lower than those of commercial Pt/C//RuO_2 system (1.573 and 1.634 V, respectively) or many other reported systems. At the same time, this two-electrode system exhibits excellent durability during the electrocatalytic water splitting. The N-doped $NiMoO_4/Ni_3N$ heterostructure could be a promising candidate for the efficient HER electrocatalyst in future practical applications.

ASSOCIATED CONTENT

Supporting Information

SEM images of Ni foam, electrodeposited $Ni(OH)_2$, N-doped $NiMoO_4/Ni(OH)_2$ composite; LSV curves of $NiMoO_4$, N-doped $NiMoO_4$ and N-doped $NiMoO_4/Ni_3N$ heterostructure with different loading amount of Ni_3N; EIS spectra of the Ni_3N, N-doped $NiMoO_4$ and N-doped $NiMoO_4/Ni_3N$ at -120 mV; CVs of $NiMoO_4$-NF, Ni_3N-NF, N-doped $NiMoO_4$ and N-doped $NiMoO_4/Ni_3N$ heterostructure at various scan rates; XPS spectra of pristine $NiMoO_4$ and N-doped $NiMoO_4$; XPS spectra, XRD pattern and SEM images of N-doped $NiMoO_4/Ni_3N$ heterostructure after 3000 continuous CV cycles; Total and partial DOS for pristine $NiMoO_4$ and N-doped $NiMoO_4$; XRD pattern, SEM images and LSV result of OER activity of the NiFe-LDH on Ni foam; Stability test of N-doped $NiMoO_4/Ni_3N$ heterostructure in more higher concentration of KOH (2.5 M and 5.0 M); Comparison of HER performance for the N-doped $NiMoO_4/Ni_3N$ heterostructure with other reported HER electrocatalysts; Comparison of the overall water splitting performance with other reported systems.

AUTHOR INFORMATION

Corresponding Author

*E-mail: pengwangicm@sdu.edu.cn

∇X.L. and Y.G. contributed equally.

Notes

There are no conflicts to declare.

ACKNOWLEDGMENTS

This work was financially supported by a research grant from the National Natural Science Foundation of China (No. 51602179, 21333006, 21573135 and 11374190), and the National Basic Research Program of China (973 Program, No. 2013CB632401), Recruitment Program for Young Professionals, China and Taishan Scholar Foundation of Shandong Province, China. Work at the Center for Nanoscale Materials, an Office of Science user facility, was supported by the U.S. Department of Energy, Office of Science, Office of Basic Energy Sciences (contract no. DE-AC02-06CH11357). Major special projects of Shandong Province, China (public welfare: 2019GGX103026).

REFERENCES

(1) Han, X.; Wu, X.; Deng, Y.; Liu, J.; Lu, J.; Zhang, C.; Hu, W. Ultrafine Pt Nanoparticle-Decorated Pyrite-Type CoS_2 Nanosheet Arrays Coated on Carbon Cloth as a Bifunctional Electrode for Overall Water Splitting. Adv. Energy Mater. 2018, 8, 1800935.

(2) Holladay, J. D.; Hu, J.; King, D.; Wang, Y. An Overview of Hydrogen Production Technologies. Catal. Today 2009, 139, 244-260.

(3) Liu, X. L.; Lv, X. S.; Wang, P.; Zhang, Q. Q.; Huang, B. B.; Wang, Z. Y.; Liu, Y. Y.; Zheng, Z. K.; Dai, Y. Improving the HER Activity of Ni_3FeN to Convert the

Superior OER Electrocatalyst to An Efficient Bifunctional Electrocatalyst for Overall Water Splitting by Doping with Molybdenum. Electrochim. Acta 2020, 333, 135488.

(4) Shi, Y. M.; Zhang, B. Recent Advances in Transition Metal Phosphide Nanomaterials: Synthesis and Applications in Hydrogen Evolution Reaction. Chem. Soc. Rev. 2016, 45, 1529-1541.

(5) Chen, G. B.; Wang, T.; Zhang, J.; Liu, P.; Sun, H. J.; Zhuang, X. D.; Chen, M. W.; Feng, X. L. Accelerated Hydrogen Evolution Kinetics on NiFe-Layered Double Hydroxide Electrocatalysts by Tailoring Water Dissociation Active Sites. Adv. Mater. 2018, 30, 1706279.

(6) Esposito, D. V.; Hunt, S. T.; Stottlemyer, A. L.; Dobson, K. D.; McCandless, B. E.; Birkmire, R. W.; Chen, J. G. Low-Cost Hydrogen-Evolution Catalysts Based on MonolayerPlatinum on Tungsten Monocarbide Substrates. Angew. Chem. Int. Ed. 2010, 49, 9859-9862.

(7) Liu, X.; Wang, P.; Zhang, Q.; Huang, B.; Wang, Z.; Liu, Y.; Zheng, Z.; Dai, Y.; Qin, X.; Zhang, X. Synthesis of MoS_2/Ni_3S_2 Heterostructure for Efficient Electrocatalytic Hydrogen Evolution Reaction through Optimizing the Sulfur Sources Selection. Appl. Surf. Sci. 2018, 459, 422-429.

(8) Yu, Z.; Duan, Y.; Gao, M.; Lang, C.; Zheng, Y.; Yu, S. A One-Dimensional Porous Carbon-Supported Ni/ Mo_2C Dual Catalyst for Efficient Water Splitting. Chem. Sci. 2017, 8, 968-973.

(9) Wang, H.; Ouyang, L.; Zou, G.; Sun, C.; Hu, J.; Xiao, X.; Gao, L. Optimizing MoS_2 Edges by Alloying Isovalent W for Robust Hydrogen Evolution Activity. ACS Catal. 2018, 8, 9529-9536.

(10) Feng, L.; Yu, G.; Wu, Y.; Li, G.; Li, H.; Sun, Y.; Asefa, T.; Chen, W.; Zou, X. High-Index Faceted Ni_3S_2 Nanosheet Arrays as Highly Active and Ultrastable Electrocatalysts for Water Splitting. J. Am. Chem. Soc. 2015, 137, 14023-14026.

(11) Faber, M. S.; Dziedzic, R.; Lukowski, M. A.; Kaiser, N. S.; Ding, Q.; Jin, S. High-Performance Electrocatalysis Using Metallic Cobalt Pyrite (CoS_2) Micro- and Nanostructures. J. Am. Chem. Soc. 2014, 136, 10053-10061.

(12) Zhang, Y. Q.; Ouyang, B.; Xu, J.; Chen, S.; Rawat, R. S.; Fan, H. J. 3D Porous

Hierarchical Nickel-Molybdenum Nitrides Synthesized by RF Plasma as Highly Active and Stable Hydrogen-Evolution-Reaction Electrocatalysts. Adv. Energy Mater. 2016, 6, 1600221.

(13) Liu, T. T.; Li, M.; Jiao, C. L.; Hassan, M.; Bo, X. J.; Zhou, M.; Wang, H. L. Design and Synthesis of Integrally Structured Ni_3N Nanosheets/Carbon Microfibers/Ni_3N Nanosheets for Efficient Full Water Splitting Catalysis. J. Mater. Chem. A 2017, 5, 9377-9390.

(14) Zhang, B.; Xiao, C. H.; Xie, S. M.; Liang, J.; Chen, X.; Tang, Y. H. Iron−Nickel Nitride Nanostructures in Situ Grown on Surface-RedoxEtching Nickel Foam: Efficient and Ultrasustainable Electrocatalysts for Overall Water Splitting. Chem. Mater. 2016, 28, 6934-6941.

(15) Ma, X. X.; Chang, Y. Q.; Zhang, Z.; Tang, J. L. Forest-Like NiCoP@Cu_3P Supported on Copper Foam as A Bifunctional Catalyst for Efficient Water Splitting. J. Mater. Chem. A 2018, 6, 2100-2106.

(16) Wang, X. D.; Chen, H. Y.; Xu, Y. F.; Liao, J. F.; Chen, B. X.; Rao, H. S.; Kuang, D. B.; Su, C. Y. Self-Supported $NiMoP_2$ Nanowires on Carbon Cloth as An Efficient and Durable Electrocatalyst for Overall Water Splitting. J. Mater. Chem. A 2017, 5, 7191-7199.

(17) Liu, Q.; Gu, S.; Li, C. M. Electrodeposition of Nickele-Phosphorus Nanoparticles Film as A Janus Electrocatalyst for Electro-Splitting of Water. J. Power Sources 2015, 299, 342-346.

(18) Yan, X. D.; Tian, L. H.; He, M.; Chen, X. B. Three-Dimensional Crystalline/Amorphous Co/Co_3O_4 Core/Shell Nanosheets as Efficient Electrocatalysts for the Hydrogen Evolution Reaction. Nano Lett. 2015, 15, 6015-6021.

(19) Yan, X. D.; Tian, L. H.; Atikins, S.; Liu, Y.; Murowchick, J.; Chen, X. B. Converting $CoMoO_4$ into CoO/MoO_x for Overall Water Splitting by Hydrogenation. ACS Sustainable Chem. Eng., 2016, 4, 3743-3749.

(20) Ou, Y. Q.; Tian, W. Q.; Liu, L.; Zhang, Y. H.; Xiao, P. Bimetallic $Co_2Mo_3O_8$ Suboxides Coupled with Conductive Cobalt Nanowires for Efficient and Durable Hydrogen Evolution in Alkaline Electrolyte. J. Mater. Chem. A 2018, 6, 5217-5228.

(21) Lu, W. B.; Liu, T. T.; Xie, L. S.; Tang, C.; Liu, D. N.; Hao, S.; Qu, F. L.; Du, G.; Ma, Y. J.; Asiri, A. M.; Sun, X. P. In Situ Derived Co-B Nanoarray: A High-Efficiency and Durable 3D Bifunctional Electrocatalyst for Overall Alkaline Water Splitting. Small 2017, 13, 1700805.

(22) Gupta, S.; Patel, N.; Fernandes, R.; Hanchate, S.; Miotello, A.; Kothari, D. C. Co-Mo-B Nanoparticles as A Non-Precious and Efficient Bifunctional Electrocatalyst for Hydrogen and Oxygen Evolution. Electrochim. Acta 2017, 232, 64-71.

(23) Zhang, J.; Wang, T.; Liu, P.; Liu, S. H.; Dong, R. H.; Zhuang, X. D.; Chen, M. W.; Feng, X. L. Engineering Water Dissociation Sites in MoS_2 Nanosheets for Accelerated Electrocatalytic Hydrogen Production. Energy Environ. Sci. 2016, 9, 2789-2793.

(24) Chen, Z. Y.; Song, Y.; Cai, J. Y.; Zheng, X. S.; Han, D. D.; Wu, Y. S.; Zang, Y. P.; Niu, S. W.; Liu, Y.; Zhu, J. F.; Liu, X. J.; Wang, G. M. Tailoring the d-Band Centers Enables Co_4N Nanosheets to Be Highly Active for Hydrogen Evolution Catalysis. Angew. Chem. Int. Ed. 2018, 57, 5076-5080.

(25) Yan, J. Q.; Li, L.; Ji, Y. J.; Li, P.; Kong, L. Q.; Cai, X. D.; Li, Y. Y.; Ma, T. Y.; Liu, S. Z. Nitrogen-Promoted Molybdenum Dioxide Nanosheets for Electrochemical Hydrogen Generation. J. Mater. Chem. A 2018, 6, 12532-12540.

(26) Xin, X.; Huang, D. K.; Fu, Y. Q.; Wen, M.; Jiang, X. X.; Lv, X. W.; Li, M.; Gao, L.; Liu, S. S.; Wang, M. K.; Zhao, C.; Shen, Y. Engineering NiS/Ni_2P Heterostructures for Efficient Electrocatalytic Water Splitting. ACS Appl. Mater. Interfaces, 2018, 10, 4689-4696.

(27) Zeng, L. Y.; Sun, K.; Wang, X. B.; Liu, Y. Q.; Pan, Y.; Liu, Z.; Cao, D. W.; Song, Y.; Liu, S. H.; Liu, C. G. Three-Dimensional-Networked Ni_2P/Ni_3S_2 Heteronanoflake Arrays for Highly Enhanced Electrochemical Overall-Water-Splitting Activity. Nano Energy 2018, 51, 26-36.

(28) Liu, X. L.; Lv, X. S.; Wang, P.; Zhang, Q. Q.; Huang, B. B.; Wang, Z. Y.; Liu, Y. Y.; Zheng, Z. K.; Dai, Y. The Synergistic Effect of Light Irradiation and Interface Engineering of the $Co(OH)_2/MoS_2$ Heterostructure to Realize the Efficient Alkaline Hydrogen Evolution Reaction. Electrochim. Acta 2019, 299, 618-625.

(29) Tian, X. D.; Li, X.; Yang, T.; Wang, K.; Wang, H. B.; Song, Y.; Liu, Z. J.; Guo, Q. G. Porous Worm-Like $NiMoO_4$ Coaxially Decorated Electrospun Carbon Nanofiber as Binder-Free Electrodes for High Performance Supercapacitors and Lithium-ion Batteries. Appl. Surf. Sci. 2018, 434, 49-56.

(30) Reddy, A. E.; Anitha, T.; Gopi, C. V. V. M.; Rao, S. S.; Kim, H. J. $NiMoO_4$@$NiWO_4$ Honeycombs as A High Performance Electrode Material for Supercapacitor Applications. Dalton Trans. 2018, 47, 9057-9063.

(31) Xie, L. S.; Qu, F. L.; Liu, Z.; Ren, X.; Hao, S.; Ge, R. X.; Du, G.; Asiri, A. M.; Sun, X. P.; Chen, L. In Situ Formation of A 3D Core/Shell Structured Ni_3N@Ni–Bi Nanosheet Array: An Efficient Nonnoble-Metal Bifunctional Electrocatalyst toward Full Water Splitting under Near-Neutral Conditions. J. Mater. Chem. A 2017, 5, 7806-7810.

(32) Ren, W. J.; Guo, D.; Zhuo, M.; Guan, B. K.; Zhang, D.; Li, Q. H. $NiMoO_4$@$Co(OH)_2$ Core/Shell Structure Nanowire Arrays Supported on Ni Foam for High-Performance Supercapacitors. RSC Adv. 2015, 5, 21881-21887.

(33) Yu, Y.; Gao, W. Y.; Shen, Z. X.; Zheng, Q.; Wu, H.; Wang, X.; Song, W. G.; Ding, K. J. A Novel Ni_3N/Graphene Nanocomposite as Supercapacitor Electrode Material with High Capacitance and Energy Density. J. Mater. Chem. A 2015, 3, 16633-16641.

(34) Wu, A. P.; Xie, Y.; Ma, H.; Tian, C. G.; Gu, Y.; Yan, H. J.; Zhang, X. M.; Yang, G. Y.; Fu, H. G. Integrating the Active OER and HER Components as the Heterostructures for the Efficient Overall Water Splitting. Nano Energy 2018, 44, 353-363.

(35) Gao, D. Q.; Zhang, J. Y.; Wang, T. T.; Xiao, W.; Tao, K.; Xue, D. S.; Ding, J. Metallic Ni_3N Nanosheets with Exposed Active Surface Sites for Efficient Hydrogen Evolution. J. Mater. Chem. A 2016, 4, 17363-17369.

(36) An, L.; Feng, J.; Zhang, Y.; Wang, R.; Liu, H. W.; Wang, G. C.; Cheng, F. Y.; Xi, P. X. Epitaxial Heterogeneous Interfaces on N-$NiMoO_4$/NiS_2 Nanowires/Nanosheets to Boost Hydrogen and Oxygen Production for Overall Water Splitting. Adv. Funct. Mater. 2019, 29, 1805298.

(37) Bao, J.; Zhang, X.; Fan, B.; Zhang, J.; Zhou, M.; Yang, W.; Hu, X.; Wang, H.; Pan, B.; Xie, Y. Ultrathin Spinel-Structured Nanosheets Rich in Oxygen Deficiencies for Enhanced Electrocatalytic Water Oxidation. Angew. Chem. Int. Ed. 2015, 54, 7399 -7404.

(38) Zhang, K. Y.; Xiao, W.; Li, J. Y.; Liu, J. G.; Yan, C. W. Two-step Preparation of Porous Nickel-sulfur Electrode for Hydrogen Evolution in Alkaline Water Electrolysis. Electrochim. Acta 2017, 228, 422-427.

(39) Zheng, Y. R.; Gao, M. R.; Yu, Z. Y.; Gao, Q.; Gao, H. L.; Yu, S. H. Cobalt Diselenide Nanobelts Grafted on Carbon Fiber Felt: An Efficient and Robust 3D Cathode for Hydrogen Production. Chem. Sci. 2015, 6, 4594-4598.

(40) Yang, Y. Q.; Zhang, K.; Lin, H. L.; Li, X.; Chan, H. C.; Yang, L. C.; Gao, Q. S. MoS2−Ni3S2 Heteronanorods as Efficient and Stable Bifunctional Electrocatalysts for Overall Water Splitting. ACS Catal. 2017, 7, 2357-2366.

(41) Zhang, B.; Liu, J.; Wang, J. S.; Ruan, Y. J.; Ji, X.; Xu, K.; Chen, C.; Wan, H. Z.; Miao, L.; Jiang, J. J. Interface Engineering: The $Ni(OH)_2/MoS_2$ Heterostructure for Highly Efficient Alkaline Hydrogen Evolution. Nano Energy 2017, 37, 74-80.

(42) Gao, M.; Chen, L. L.; Zhang, Z. H.; Sun, X. P.; Zhang, S. S. Interface Engineering of the $Ni(OH)_2$-Ni_3N Nanoarray Heterostructure for the Alkaline Hydrogen Evolution Reaction. J. Mater. Chem. A 2018, 6, 833-836.

(43) Liu, J.; Wang, J. S.; Zhang, B.; Ruan, Y. J.; Wan, H. Z.; Ji, X.; Xu, K.; Zha, D. C.; Miao, L.; Jiang, J. J. Mutually Beneficial Co_3O_4@MoS_2 Heterostructures as A Highly Efficient Bifunctional Catalyst for Electrochemical Overall Water Splitting. J. Mater. Chem. A 2018, 6, 2067-2072.

(44) Muthurasu, A.; Maruthapandian, V.; Kim, H. Y. Metal-Organic Framework Derived Co_3O_4/MoS_2 Heterostructure for Efficient Bifunctional Electrocatalysts for Oxygen Evolution Reaction and Hydrogen Evolution Reaction. Appl. Catal., B 2019, 248, 202-210.

(45) Xiong, T.; Li, G. F.; Young, D. J.; Tan, Z. Y.; Yin, X. H.; Mi, Y.; Hu, F. L. In-Situ Surface-Derivation of Ni-Mo Bimetal Sulfides Nanosheets on Co_3O_4 Nanoarrays as An Advanced Overall Water Splitting Electrocatalyst in Alkaline

Solution. J. Alloys Compd. 2019, 791, 328-335.

(46) Li, X. M.; Hao, X. G.; Wang, Z. D.; Abudula, A.; Guan, G. Q. In-Situ Intercalation of NiFe LDH Materials: An Efficient Approach to Improve Electrocatalytic Activity and Stability for Water Splitting. J. Power Sources 2017, 347, 193-200.

(47) Liu, J.; Wang, J.; Zhang, B.; Ruan, Y.; Lv, L.; Ji, X.; Xu, K.; Miao, L.; Jiang, J. Hierarchical $NiCo_2S_4$@NiFe LDH Heterostructures Supported on Nickel Foam for Enhanced Overall-Water-Splitting Activity. ACS Appl. Mater. Interfaces 2017, 9, 15364-15372.

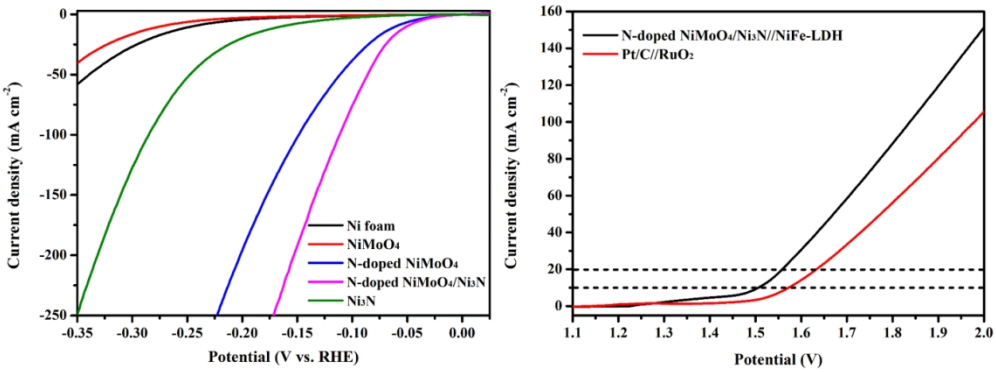

237x87mm (150 x 150 DPI)